An Experimental Study on Microwave Imaging of Breast Cancer with the use of Tumor Phantom

Mustafa B. Bicer and Ali Akdagli

Department of Electrical and Electronics Engineering
Mersin University, Mersin, 33343, Turkey
mbbicer@mersin.edu.tr, akdagli@mersin.edu.tr

Abstract ─ Nowadays, breast cancer is the most common type of the cancer among women's diseases. It is the leading cause of death after cardiovascular diseases. Due to risk of uncontrolled reproduction and propagation of the cancer cells, early diagnosis has a crucial importance. Microwave imaging (MWI) is an evolving method and has a variety of advantages such as operating at lower frequencies with a lower power, cost-effectiveness, and providing comfortable measurements without contact. In this paper, an experimental study on microwave imaging of breast cancer with the use of tumor phantom is presented. For this purpose, an experimental setup containing sand, screw and tumor phantom is prepared as replacement of real tissue. Two-dimensional inverse synthetic aperture radar (ISAR) method is used in handling the scattered electric field data from the measurement setup. Inverse radon transform (IRT) method is then utilized to extract the image of the measured scattering electric field data. The resultant images show that the microwave imaging method can be successfully used together with IRT for the breast cancer problem.

Index Terms ─ Breast cancer, breast phantom, imaging algorithm, microwave imaging, radar-based imaging.

I. INTRODUCTION

At present, cancer is the disease having the highest mortality rate after cardiovascular diseases and the breast cancer is the leading one among the female population. Early detection and diagnosis of the breast cancer is a key factor due to having 95% survival rate in its early stages. There are various primary modalities for breast cancer imaging and diagnosis such as x-ray mammography, magnetic resonance imaging (MRI) and ultrasound imaging (USI) [1,2]. However, there are significant disadvantages of these methods such as the use of x-rays and compression requirements of the breast for x-ray mammography; expensiveness and low specificity of MRI and the need of pressurizing the breast while applying USI. On the other hand, microwave imaging having advantages such as providing independent information about tumor tissue, having a wide application area, and high sensitivity and specificity is gaining a high interest by the researchers and pharmaceutical companies. The use of microwaves in breast cancer imaging is attracting researcher's attention and consequently many related studies are reported in the literature [2–20]. Microwave imaging (MWI) is a promising alternative to x-ray mammography since it has many advantages such as low-cost, using non-ionizing microwave, no need to compress the breast, portable fabrication and safety of using low power levels [3]. Microwave tomography and radar-based microwave imaging are two main methods that illuminate the breast with signals in microwave band and measure the backscattered or transmitted signals. The radar-based MWI (RBMWI) is especially widely researched method that provides simple and powerful image reconstruction algorithms [11–24]. The microwave signals scatter from each different dielectric interface because of the contrast in the dielectric constants and the scattered signals contain physical information such as size and distance of the scattering object. RBMWI technique uses the difference of permittivities between healthy and malignant tissues over the microwave frequency range to reconstruct the breast image map from scattering signals [2–20]. In the literature, there are several theoretical and experimental studies on radar-based imaging methods such as confocal microwave imaging [7,11], statistical microwave imaging [8], multistatic adaptive microwave imaging [9], field mapping algorithm [10], dynamic microwave imaging [17], hybrid reconstruction [18], multistatic delay-and-sum [19], microwave imaging with stochastic optimization [20]. In [22], a compact bowtie antenna with cavity operating in the range between 2 – 4 GHz is designed for microwave breast cancer imaging and two-dimensional tumor scattering map was obtained. Fear *et al*. [11] used the method of confocal microwave imaging with the help of data acquired from the numerically modelled breast, and the breast tumor of 6 mm in size was imaged in three-dimensional while Li *et al*. [7] imaged the tumor of 4 mm in size in two-dimensional. In [13], experimental studies were carried out with the use of coupling liquid to

Submitted On: April 12, 2017
Accepted On: September 10, 2017

provide the matching between the breast skin and the antenna array. References [8] and [10] present the methods of statistical microwave imaging and field mapping algorithm to obtain the two-dimensional screening map with several experimental results, respectively. In order to exploit the advantages of array of antennas, a monopole antenna array of 16-elements in the liquid coupling with the breast skin was proposed in [14]. Although there are many methods given above for imaging, they have been used with their own benefits and limitations but none of them fulfill all of the requirements. Therefore, microwave imaging methods based on theoretical, experimental and also simulation have been continuously developed by using the antenna systems including monostatic, bi-static and array configurations. The theoretical and simulation approaches are numerically handled by ignoring the effects of physical conditions such as noise, multipath effects, antenna and cable losses and intrinsic errors. Suggestion of liquid usage for coupling between the breast and the antenna results in uncomfortable measurement for the patient. Antenna arrays provide fast data acquirement at the expense of system complexity.

In this work, microwave imaging for breast cancer detection is carried out experimentally by using the monostatic antenna without coupling liquid. The reconstruction method of inverse radon transform (IRT) [25] is merged with the inverse synthetic aperture radar (ISAR) [26] principle without introducing the antenna array. IRT, as an imaging method, is simple and easy to use and implement. With the use of ISAR principle, an individual antenna acts as if it were an array of antennas. In this work, to take advantages of both IRT and ISAR, electrical field scattering data from the phantom were experimentally acquired by ISAR and the resultant image including the representative tumors was successfully reconstructed with IRT method.

The paper is organized as follows: at first, fundamentals of monostatic ISAR principle are explained. The reconstructed images are then given for four different scenarios in the section of experimental results. In conclusion section, the achieved results are briefly described.

II. INVERSE SYNTHETIC APERTURE RADAR (ISAR) PRINCIPLE

According to the monostatic ISAR principle, the phantom is illuminated with electromagnetic waves and rotated on its axis in such a way that it is concentric with the illuminating antenna. The reflected electromagnetic waves are measured with an antenna [26]. Principle of two dimensional monostatic ISAR imaging is shown in Fig. 1.

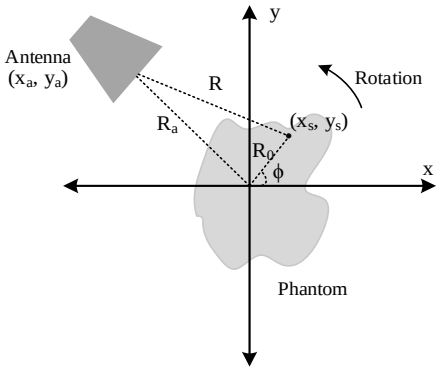

Fig. 1. Two dimensional monostatic ISAR imaging principle.

The scattering field vector in frequency domain $E_s[f,\phi]$ is calculated as [26]:

$$E_s[f,\phi] = A_0 e^{-j\left(\frac{4\pi f}{v}\right)R(\phi)}, \quad (1)$$

where f, A_0, R and ϕ terms represent a frequency vector, the amplitude of the electric field, the Euclidean distance between the antenna and the phantom and the cylindrical angle, respectively. The phase velocity of the wave in the medium $v = \frac{c}{\sqrt{\varepsilon_r}}$ and ε_r denotes the dielectric constant of the medium. The Euclidean distances are calculated as in [26]:

$$R = \sqrt{\left(\left|x_a - R_0\cos(\phi)\right|\right)^2 + \left(\left|y_a - R_0\sin(\phi)\right|\right)^2}, \quad (2)$$

while R_0 denote the tumor distance relative to the origin of the breast, (x_a, y_a) represents the position of the antenna. For the sake of simplicity, the whole experimental setup is assumed to be homogeneous and the phantom consists of discrete points. The values of the parameters are given in Table 1 and the experimental setup is illustrated in Fig. 2.

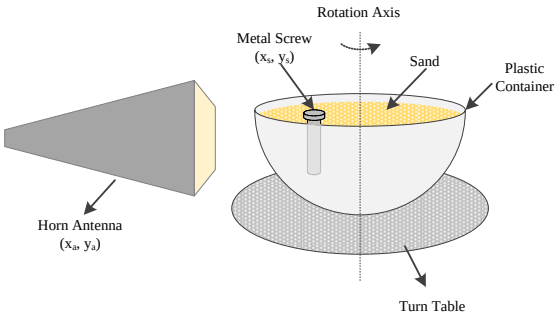

Fig. 2. Measurement setup.

Table 1: Values for measurement parameters

Parameter	Value			
Power (mW)	1			
Start frequency (GHz)	2			
Stop frequency (GHz)	8			
Frequency count	601			
Foam container radius (cm)	7			
Antenna distance (cm)	12			
Rotation angle increment (degree)	1			
Screw dimension (cm x cm)*	1 x 5			
	Locations (r, ϕ) for Scenarios			
	#1	#2	#3	#4
Screw	(0,0°)	(4,180°)	(5,190°)	–
Phantom	–	–	–	(3,170°)

**Screw dimension (Diameter x Width)*

The antenna is located R_a distance from the center of the foam container. The container is rotated around the z-axis and at each angle, the scattered field from each discrete point of the phantom is summed according to:

$$E_{total}(r,\phi)=\int_0^{2\pi}\int_0^{R} A_0 e^{-j\left(\frac{4\pi f}{v}\right)r}\,dr d\phi, \qquad (3)$$

where ϕ and r represent the angle difference between the actual and the range between the antenna and the scattering object, respectively. The electric field matrix obtained with the use of Eq. (3) contains information about the skin and tumor points. When the measured data are analyzed, it is understood that there are strong radiations from the tumor tissue(s) and skin. In addition, background subtraction was applied to highlight the effect of the radiations. Background subtraction is defined as:

$$E = E_{total} - E_{calibration}, \qquad (4)$$

where $E_{calibration}$ represents the electric field data in the stage of only sand filled container. Then, the size of data is increased by applying zero-padding method so as to obtain the better quality for images, as follows:

$$E(r,\phi)=\begin{cases} E(r,\phi), & r=0,...,N-1 \\ 0, & r=N,...,M-1 \end{cases}, \qquad (5)$$

where N and M represent the lengths of the measured electric field data and the target data, respectively. The resultant data is filtered by using Binomial filter. The coefficients of the Binomial filter are calculated by:

$$h=\sum_{j=1}^{J}(h*cc), \qquad (6)$$

where h, J and cc denote filter coefficients of the filter, limit of the iteration and a constant coefficient, respectively. In this study, cc is selected as [0.5 0.5] and the initial value of the h is selected as same as cc while J is set to 571. The IRT method is then utilized on the resultant data to reconstruct the resultant image [25]. The pixel value of image G using inverse radon transform is defined as,

$$G(x,y)=\int_0^{2\pi} E(x\cos(\phi)+y\sin(\phi),\phi)\,d\phi, \qquad (7)$$

where x and y define the location of the image and ϕ is the cylindrical angle aforementioned in Eq. (2). E in Eq. (7) is an array consist of electric field data depending on frequency values in start and stop frequencies accordingly. Since the measurement setup is based on the monostatic imaging, the upper limit of ϕ is 2π rather than π. The flowchart summarizing the applied procedures carried out in this work is given in Fig. 3.

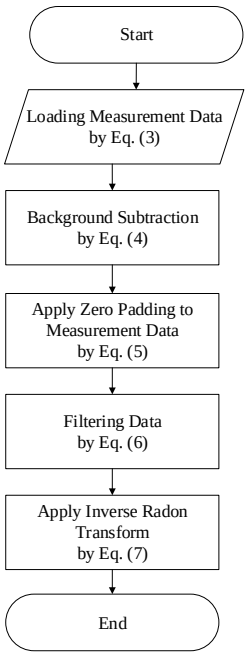

Fig. 3. Flowchart of the microwave imaging procedure used in this work.

III. EXPERIMENTAL RESULTS

In this study, breast tumor tissue phantom proposed by Ortega-Palacios *et al*. [27] is formed to be used in measurements for microwave imaging. For measurements, the phantom is placed in a container filled with sand. Results of the measured permittivity for the sand and phantom from 2 to 8 GHz frequency range are given in Fig. 4.

In medical applications, biological tissues show lossy medium properties because of their conductivity. With the rise of frequency, the penetration depth of the electromagnetic wave begins to decrease. For this reason, the optimal frequency range should be chosen so that the waveguide can penetrate to achieve an optimal imaging. The UWB band is acceptable to ensure optimal imaging.

It can be seen from the Fig. 4 that the permittivity of sand is remained constant at almost 2 while the permittivity of the tumor phantom is decreasing monotonously from 70 to 59 in the range of 2 to 8 GHz. The dielectric constant values of the tumor and healthy breast tissue are given in Table 2. These values are computed by using the 4-Cole-Cole Model [28].

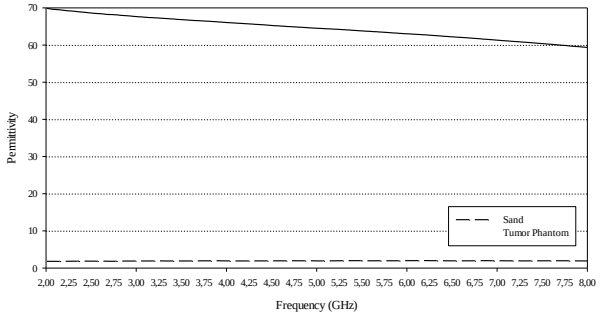

Fig. 4. Measured permittivity data of the sand (dashed) and the tumor (solid) phantom.

Table 2: Computed dielectric constant values of real human tissues at different frequencies [26]

Tissue	Frequencies for Dielectric Constants (ε)		
	2 GHz	4 GHz	6 GHz
Breast Fat	5.232	4.839	4.462
Skin (Dry)	38.567	36.587	34.945
Skin (Wet)	43.520	40.847	38.377

In this study, the effect of skin is disregarded. As it can be seen from the Fig. 4 and Table 2, the dielectric constant value of the sand and real breast tissue is close enough, thus, sand is eligible to use in the measurement setup. Microwave imaging is based on the contrast difference between the dielectric constant value of healthy and tumor tissues. The constant difference between sand and tumor phantom is appropriate. The frequency domain measurements are performed by the help of Agilent ENA E5071B Series RF Network Analyzer at the anechoic chamber, a double-ridged horn antenna and a turntable for rotation. The return loss data of 601 frequency points from 2 GHz to 8 GHz are acquired by using the double-ridged horn antenna. The gain values of the antenna are specified as 5 dBi, 13 dBi, 15 dBi, and 16 dBi for 2 GHz, 4 GHz, 6 GHz, and 8 GHz frequencies, respectively. The use of the double-ridged horn antenna eliminates the disadvantages such as low gain and omnidirectional radiation pattern of the microstrip antennas. A foam container filled with sand is placed on a plate of a computer-controlled turntable that rotates with a precision of 1 degree. The double ridged horn antenna, operating at 2 – 26 GHz frequency band, is placed 12 cm away from the container. For the scenarios #1 – 3, a metallic screw is placed in the sand at different positions. Then, a malignant tumor phantom is placed at 3 cm away from the center of the container for scenario #4. Before beginning the scenario-related measurements, sand only filled container without screw or phantom is measured. The measurement was used in the calibration process by background subtraction method to remove ambient effects. Background subtraction process is performed by subtracting the data acquired from screwless scenario from other scenarios. After the calibration, one screw is positioned at different locations in the sand filled foam container for the next three scenarios as shown in Fig. 5.

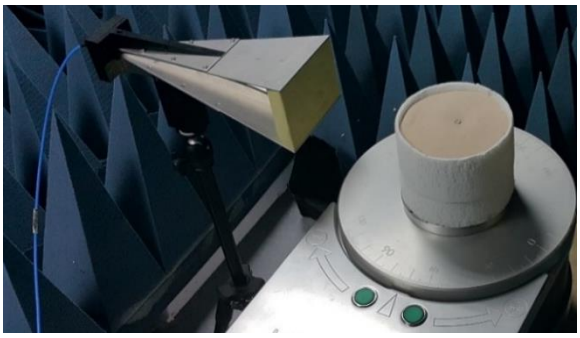

Fig. 5. Screw in sand filled foam container on the turntable.

Figure 6 (a) shows the sand filled foam container without screw or tumor phantom. The blue circle refers to the foam container. The return loss data is measured in the frequency domain. For image generation, the resultant data obtained by applying Inverse Fast Fourier Transform (IFFT) to the measured ones is used. Physical circumstances such as losses related to multiple reflections inside the foam container and the interactions between antenna and the container, and the conditions depending on filtering and other preprocessing procedures applied to can be considered as the reason for the artifacts. Some of the mentioned artifact sources can be eliminated with background subtraction procedure.

Figure 6 (b) shows the image of the screw placed in the origin of the foam container obtained after the background subtraction procedure. As it is seen from Fig. 6 (c) and Fig. 6 (d), when the screw was moved towards the edge of the container, distortions occurred in the obtained image. A sharper image could be obtained by lowering the value of the dynamic range based on logarithmic scaling, but in this study, the dynamic range is taken large enough to show possible artifacts. In addition, the larger value of the dynamic range causes the smaller objects to appear larger than their actual size. Therefore, the dynamic range value should be selected optimally. By decreasing the dynamic range value, the detection and imaging of the object can be simplified and artifacts with low amplitudes can be eliminated. Also,

postprocessing methods can be applied to remove the artifacts from the obtained image. It is assumed that the region with the highest peak value of the amplitudes is related to the scatterer. Therefore, the calculated positions are chosen to be the point at which the highest peak value is found. The more precise detection of the location can be performed by reducing the dynamic range value.

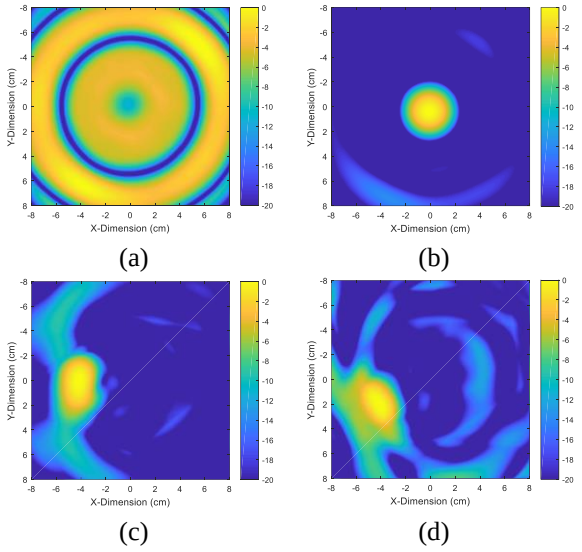

Fig. 6. (a) Sand filled foam container without screw or phantom, (b) screw positioned in the center of the foam container, (c) screw positioned 4 cm, and (d) 5 cm away from the center of the foam container.

In next scenarios, a screw is placed in various positions in the sand. As seen in Fig. 6 (b), screw is located in the center of the foam container. Then, screw is placed 4 and 5 cm away from the center, respectively, as seen from Fig. 6 (c) and Fig. 6 (d). When the screw is moved away from the center of the container, the screw resembles an ellipse-like shape. The maximum peaks are calculated as placed 4.15 cm and 4.63 cm away from the center for scenario 2 and scenario 3, respectively. Finally, the 2-cm diameter of tumor phantom is placed at the distance of 3 cm from the center of the sand filled foam container. The generated image with the use of IRT method is given in Fig. 7. The position of the tumor phantom is calculated as 3.31 cm away from the center using the Fig. 7.

Since the phantom lost water during the measurement, only one measurement could be made. The numerical results for the physical and calculated positions from the generated image are given in Table 3.

According to Table 3, the screw positions in the sand filled foam container for three scenarios are, respectively, calculated as 0.42 cm, 0.15 cm and 0.36 cm away from the initial screw positions and the phantom position is 0.31 cm different from the actual position. These deviations in approximately calculated positions on the resultant image are within acceptable ranges. The noises and position deviations shown in Fig. 6 and Fig. 7 are due to algorithm-dependent parameters, water loss of the tumor phantom during the measurement, crosstalk of the antenna, and reflections from the gap between the antenna and the container.

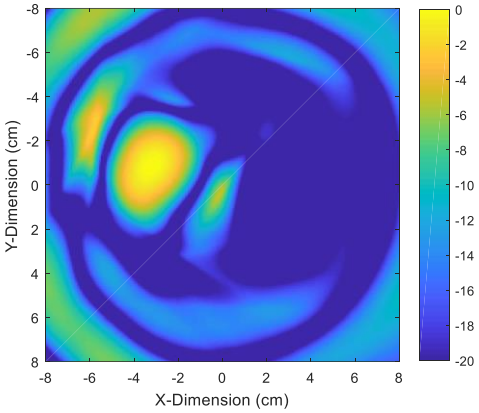

Fig. 7. Phantom positioned 3 cm away from the center of the foam container.

Table 3: The initial positions and calculated positions from the generated image

	Physical Position (r, ϕ)	Calculated Position (r, ϕ)
Screw	(0 cm, 0˚)	(0.42 cm, 0˚)
	(4 cm, 180˚)	(4.15 cm, 184˚)
	(5 cm, 205˚)	(4.63 cm, 208˚)
Tumor Phantom	(3 cm, 175˚)	(3.31 cm, 173˚)

IV. CONCLUSION

In this study, the method of IRT was utilized to reconstruct the image of the emulated breast with a malignant tumor by using the data acquired by ISAR principle. The experimental studies were carried out with four scenarios containing screw and tumor phantom at different locations. Sand and a screw were chosen in the first three scenarios because of having highly contrasted permittivity values. In the last scenario, a realistic tumor phantom was created and placed in the sand. For all scenarios, the container was illuminated by electromagnetic waves from various angles by rotating the container with turntable. Experimental measurements were taken with the use of network analyzer in frequency domain. By increasing the sample points, the image with higher resolution relatively can be reconstructed at the expense of much more elapsed measurement and processing time. The IRT algorithm was utilized to generate the radar-based microwave image of the experimental setup for the four scenarios. The resultant

images were obtained with a success and the IRT algorithm showed a good performance on breast cancer imaging with microwaves.

ACKNOWLEDGMENT

This study was supported by the Research Fund of Mersin University in Turkey with Project Number: 2017-1-TP3-2190. The authors are thankful to the Electrical and Electronics Engineering of Iskenderun Technical University for their help in the dielectric constant measurement of the tumor phantom.

REFERENCES

[1] M. Patlak, S. J. Nass, I. C. Henderson, and J. C. Lashof, Mammography and Beyond: Developing Technologies for the Early Detection of Breast Cancer, Washington, DC: National Academy Press, 2001.

[2] M. B. Bicer, A. Akdagli, and C. Ozdemir, "Breast cancer detection using inverse radon transform with microwave image technique," *23th Signal Processing and Communications Applications Conference (SIU)*, Malatya, TR, pp. 2182-2185, 2015.

[3] E. C. Fear, P. M. Meaney, and M. A. Stuchly, "Microwaves for breast cancer detection?," *IEEE Potentials*, vol. 22, no. 1, pp. 12, 2003.

[4] D. J. Kurrant, E. C. Fear, and D. T. Westwick, "Tumor response estimation in radar-based microwave breast cancer detection," *IEEE Transactions on Biomedical Engineering*, vol. 55, no. 12, pp. 2801-2811, 2008.

[5] S. K. Davis, B. D. Van Veen, S. C. Hagness, and F. Kelcz, "Breast tumor characterization based on ultrawideband microwave backscatter," *IEEE Trans. Biomed. Eng.*, vol. 55, no. 1, pp. 237-246, 2008.

[6] Y. Chen and P. Kosmas, "Detection and localization of tissue malignancy using contrast-enhanced microwave imaging: Exploring information theoretic criteria," *IEEE Trans. Biomed. Eng.*, vol. 59, no. 3, pp. 766-776, 2012.

[7] X. Li, E. J. Bond, B. D. Van Veen, and S. C. Hagness, "An overview of ultra-wideband microwave imaging via space-time beamforming for early-stage breast-cancer detection," *IEEE Antennas Propag. Mag.*, vol. 47, no. 1, pp. 19-34, 2005.

[8] S. K. Davis, H. Tandradinata, S. C. Hagness, and B. D. Van Veen, "Ultrawideband microwave breast cancer detection: A detection-theoretic approach using the generalized likelihood ratio test," *IEEE Trans. Biomed. Eng.*, vol. 52, no. 7, pp. 1237-1250, 2005.

[9] Y. Xie, B. Guo, L. Xu, J. Li, and P. Stoica, "Multistatic adaptive microwave imaging for early breast cancer detection," *IEEE Trans. Biomed. Eng.*, vol. 53, no. 8, pp. 1647-1657, 2006.

[10] G. Cheng, Y. Zhu, and J. Grzesik, "3-D microwave imaging for breast cancer," *6th European Conference on Antennas and Propagation (EUCAP)*, Prague, pp. 3672-3676, 2011.

[11] E. C. Fear, X. Li, S. C. Hagness, and M. A. Stuchly, "Confocal microwave imaging for breast cancer detection: Localization of tumors in three dimensions," *IEEE Trans. Biomed. Eng.*, vol. 49, no. 8, pp. 812-822, 2002.

[12] E. J. Bond, X. Li, S. C. Hagness, and B. D. Van Veen, "Microwave imaging via space-time beamforming for early detection of breast cancer," *IEEE Transactions on Antennas and Propagation*, vol. 51, no. 8, pp. 1690-1705, 2003.

[13] M. Klemm, I. Craddock, J. Leendertz, A. Preece, and R. Benjamin, "Experimental and clinical results of breast cancer detection using UWB microwave radar," *IEEE Antennas and Propagation Society International Symposium*, no. 1, pp. 1-4, 2008.

[14] P. M. Meaney, M. W. Fanning, T. Zhou, A. Golnabi, S. D. Geimer, and K. D. Paulsen, "Clinical microwave breast imaging - 2D results and the evolution to 3D," *Proceedings of the 2009 International Conference on Electromagnetics in Advanced Applications*, ICEAA'09, pp. 881-884, 2009.

[15] N. Irishina, M. Moscoso, and O. Dorn, "Microwave imaging for early breast cancer detection using a shape-based strategy," *IEEE Trans. Biomed. Eng.*, vol. 56, no. 4, pp. 1143-1153, 2009.

[16] H. B. Lim, N. T. T. Nhung, E.-P. Li, and N. D. Thang, "Confocal microwave imaging for breast cancer detection: Delay-multiply-and-sum image reconstruction algorithm," *IEEE Transactions on Biomedical Engineering*, vol. 55, no. 6. pp. 1697-1704, 2008.

[17] M. Klemm, I. J. Craddock, and A. Preece, "Contrast-enhanced breast cancer detection using dynamic microwave imaging," *Proceedings of the 2012 IEEE International Symposium on Antennas and Propagation*, pp. 1-2, 2012.

[18] M. Pastorino, "Hybrid reconstruction techniques for microwave imaging systems," *2010 IEEE International Conference on Imaging Systems and Techniques*, pp. 198-203, 2010.

[19] I. Ünal, B. Türetken, and Y. Çotur, "Microwave imaging of breast cancer tumor inside voxel-based breast phantom using conformal antennas," *31st URSI General Assembly and Scientific Symposium*, pp. 1-4, 2014.

[20] A. Jeremic and E. Khoshrowshahli, "Detecting breast cancer using microwave imaging and stochastic optimization," *Engineering in Medicine and Biology Society (EMBC), 2015 37th Annual International Conference of the IEEE*, pp. 89-92,

2015.
[21] R. Benjamin, I. J. Craddock, G. S. Hilton, S. Litobarski, E. McCutheon, R. Nilavalan, and G. N. Crisp, "Microwave detection of buried mines using non-contact, synthetic near-field focusing," *Radar, Sonar Navig. IEE Proc.*, vol. 148, no. 4, pp. 233-240, 2001.
[22] X. Yun, E. C. Fear, and R. H. Johnston, "Compact antenna for radar-based breast cancer detection," *IEEE Trans. Antennas Propag.*, vol. 53, no. 8, pp. 2374-2380, 2005.
[23] A. K. Alqallaf, R. K. Dib, and S. F. Mahmoud, "Microwave imaging using synthetic radar scheme processing for the detection of breast tumors," *The Applied Computational Electromagnetics Society Journal (ACES Journal)*, vol. 31, no. 2, pp. 98-105, 2016.
[24] İ. Ünal, B. Türetken, and C. Canbay, "Spherical conformal bow-tie antenna for ultra-wide band microwave imaging of breast cancer tumor," *The Applied Computational Electromagnetics Society Journal (ACES Journal)*, vol. 29, no. 2, pp. 124-133, 2014.
[25] W. M. Boerner, C. M. Ho, and B. Y. Foo, "Use of Radon's projection theory in electromagnetic inverse scattering," *IEEE Trans. Antennas Propag.*, vol. 29, no. 2, pp. 336-341, 1981.
[26] C. Ozdemir, *Inverse Synthetic Aperture Radar Imaging*. NJ: Wiley & Sons, Inc., 2012.
[27] R. Ortega-Palacios, L. Leija, A. Vera, and M. F. J. Cepeda, "Measurement of breast - Tumor phantom dielectric properties for microwave breast cancer treatment evaluation," *Program and Abstract Book - 2010 7th International Conference on Electrical Engineering, Computing Science and Automatic Control*, pp. 216-219, 2010.
[28] C. Gabriel, *Compilation of the Dielectric Properties of Body Tissues at RF and Microwave Frequencies.* U.S. Air Force Report, 1996.

Mustafa Berkan Bicer was born in 1988. In 2009, he received B.S. degree in Electrical and Electronics Engineering from Firat Universiy, Turkey. In 2012, he received M.S. degree in Electrical and Electronics Engineering from Mersin University, Turkey. He has been working as Research Engineer at Electrical and Electronics Engineering Department of Mersin University since 2009. He has been studying towards the Ph.D. degree at the same department. His current research interests include microwave imaging, antennas, microstrip antennas, computational electromagnetic, artificial intelligent and applications of optimization algorithms to electromagnetic problem such as radiation, resonance and bandwidth.

Ali Akdagli obtained the B.S., M.S. and Ph.D. degrees from Erciyes University, Kayseri, in 1995, 1997 and 2002 respectively, all in Electronic Engineering. From 2003 to 2006 he was an Assistant Professor in the Electronic Engineering Department at Erciyes University. He joined the same department at Mersin University, where he currently works as an Associate Professor. He has published more than 100 papers in journals and conference proceedings. His current research interests include evolutionary optimization techniques (genetic algorithm, ant colony optimization, differential evolution, particle swarm optimization, and artificial bee colony algorithms), artificial neural networks and their applications to electromagnetic, microwave circuits, microstrip antennas and antenna pattern synthesis problems.